

Supporting Information

Near-infrared Laser and H₂O₂ Activated Bio-nanoreactor for Enhanced Photodynamic Therapy of Hypoxic Tumor

Liming Deng^a, Danli Sheng^b, Mingzhu Liu^a, Lu Yang^c, Haitao Ran^a, Pan Li^a, Xiaojun Cai^{d*}, Yang Sun^{a*}, Zhigang Wang^{a*}

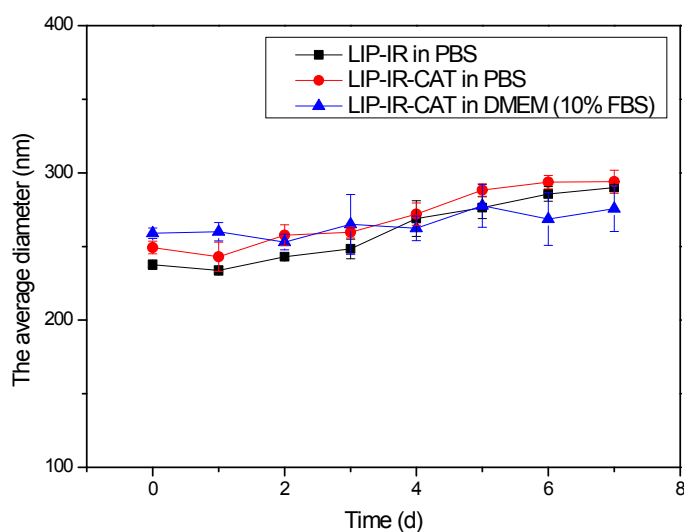


Figure S1. The average diameter change of LIP-IR and LIP-IR-CAT over 7 days measured by dynamic light scattering (DLS).

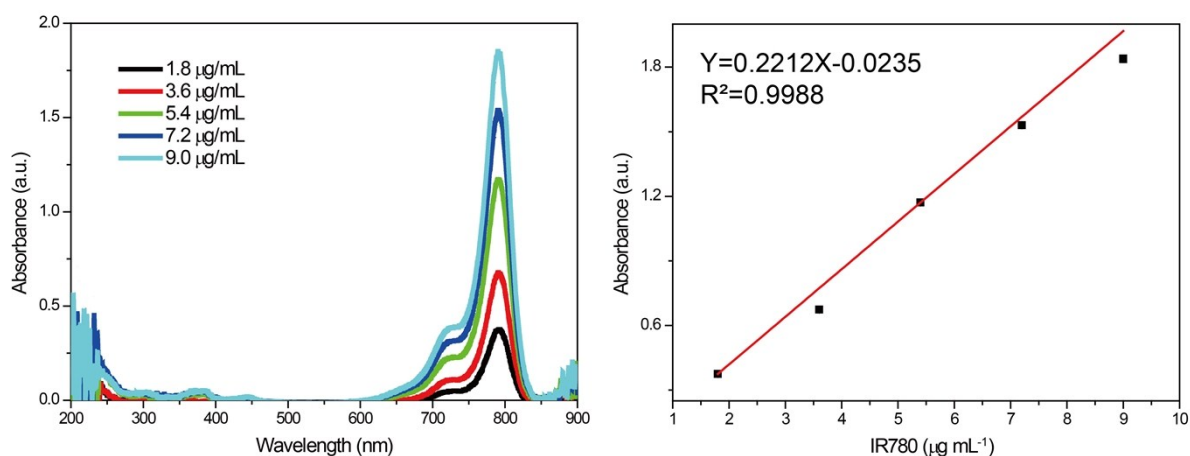


Figure S2. a) Absorbance spectra of IR780 dispersed in chloroform at various concentrations. b) The concentration-absorbance standard curve of IR780.

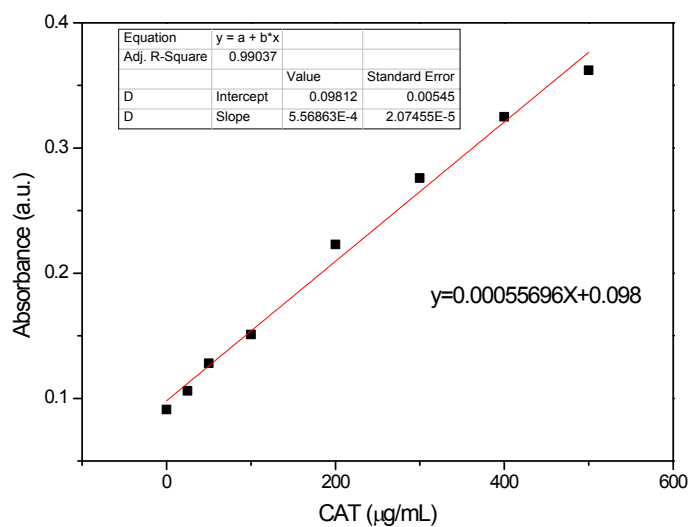


Figure S3. The concentration-absorbance standard curve of catalase by bicinchoninic acid (BCA) protein assay.

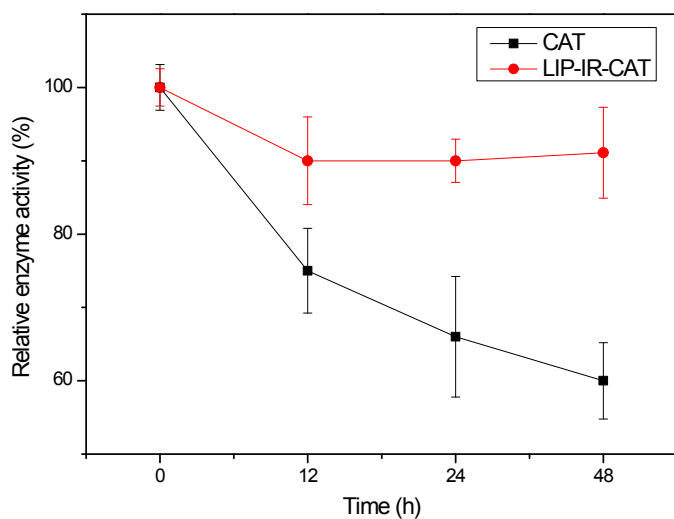


Figure S4. The relative enzyme activity of free CAT and LIP-IR-CAT after storage at 4°C.

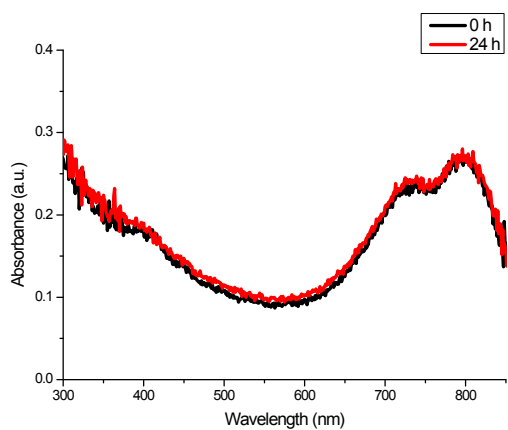


Figure S5. Absorption spectra change over time of LIP-IR-CAT at 4°C.

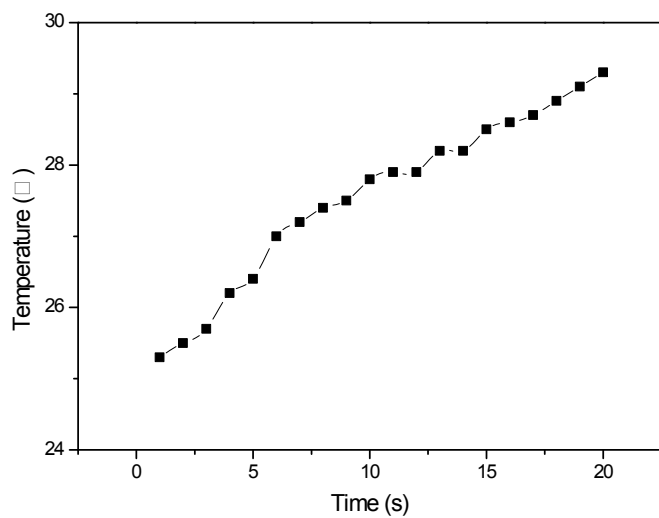


Figure S6. Temperature elevation of LIP-IR-CAT aqueous solution (200 $\mu\text{g/mL}$) with NIR laser irradiation (1W/cm^2).

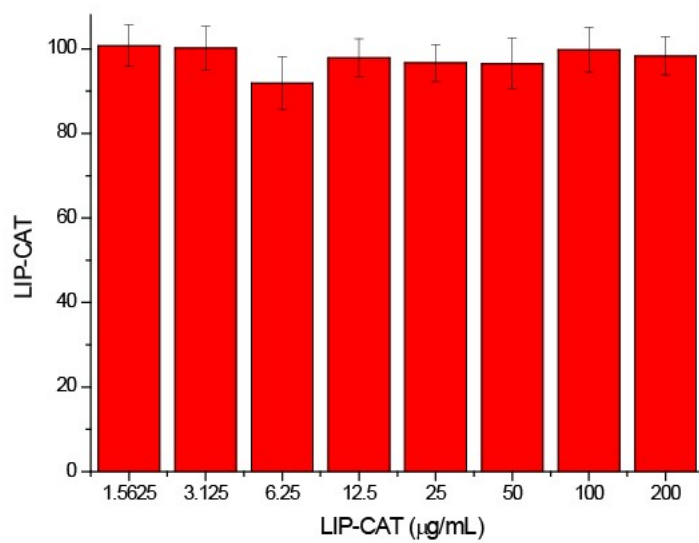


Figure S7. Cell viability of LIP-CAT after incubation with MDA-MB-231 cells for 24 h.

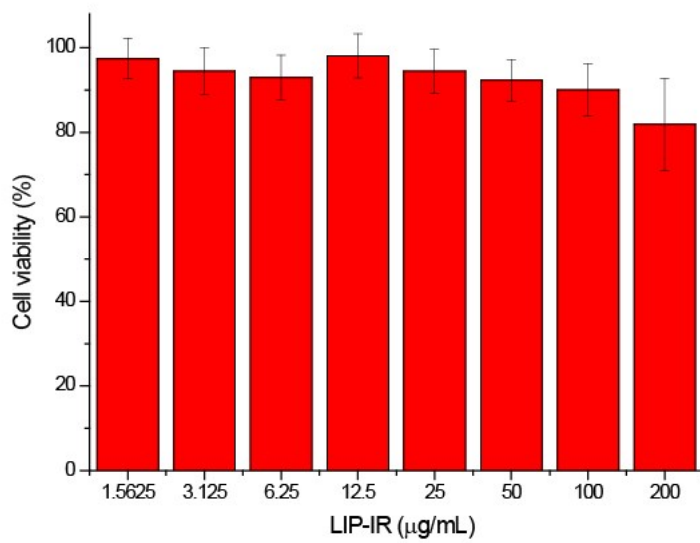


Figure S8. Cell viability of LIP-IR after incubation with MDA-MB-231 cells for 24 h.

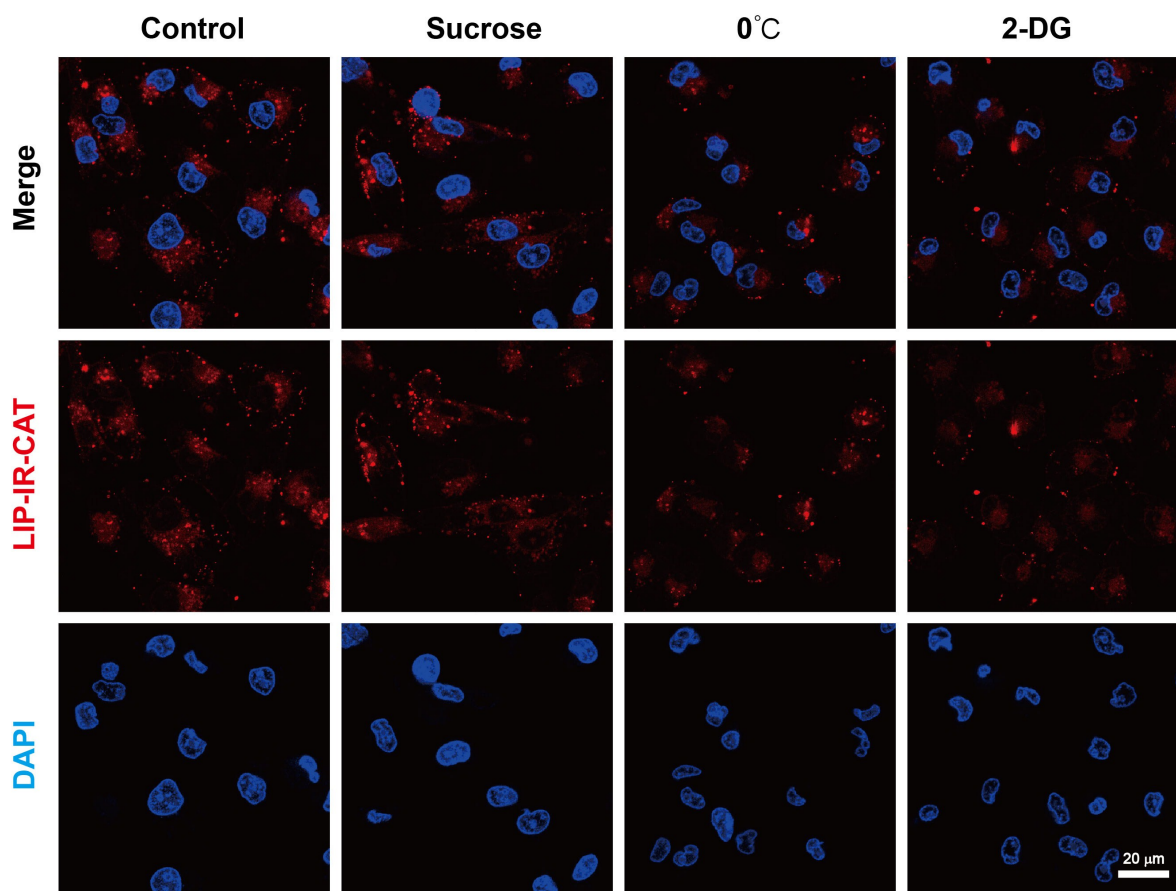


Figure S9. The role of energy metabolism and endocytosis on LIP-IR-CAT uptake. Confocal images of MDA-MB-231 cells pretreated with 2-DG, sucrose for 1 h, and 0°C for 30 min. Scale bar: 20 µm.

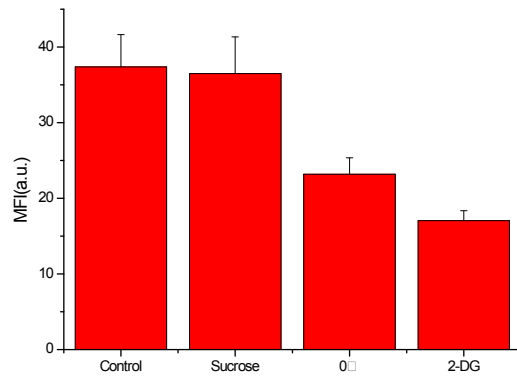


Figure S10. The quantification of mean fluorescence intensity (MFI) in MDA-MB-231 cells after various treatments. Values are the means \pm SD (n = 3).

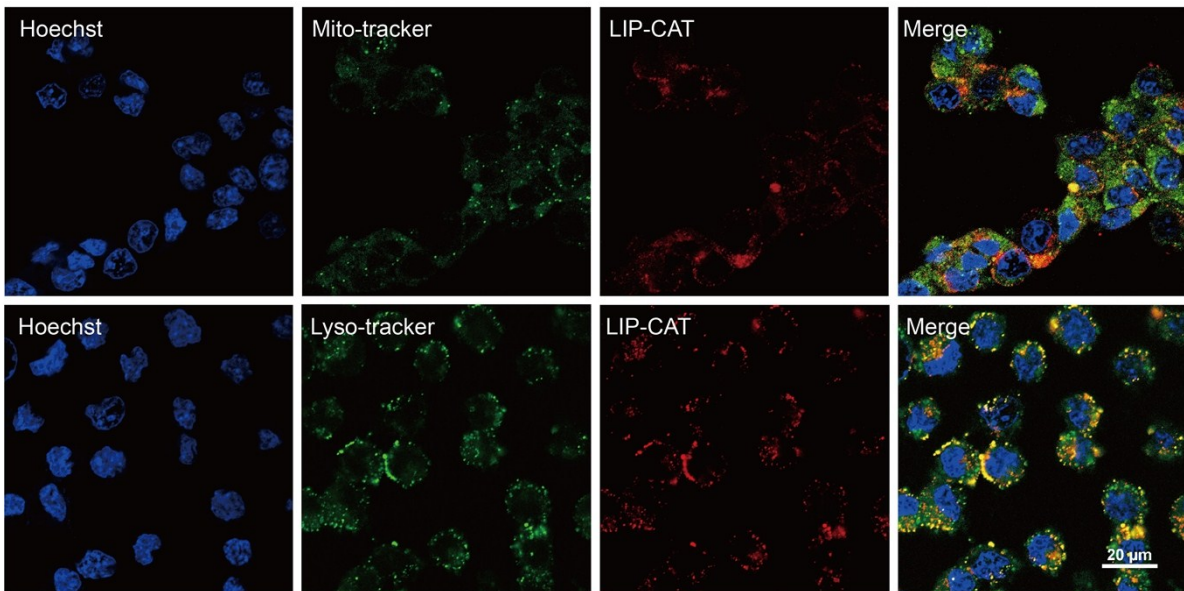


Figure S11. Confocal images of MDA-MB-231 cells incubated with DiI-labeled LIP-CAT for 1 h. Scale bar: 20 μ m.

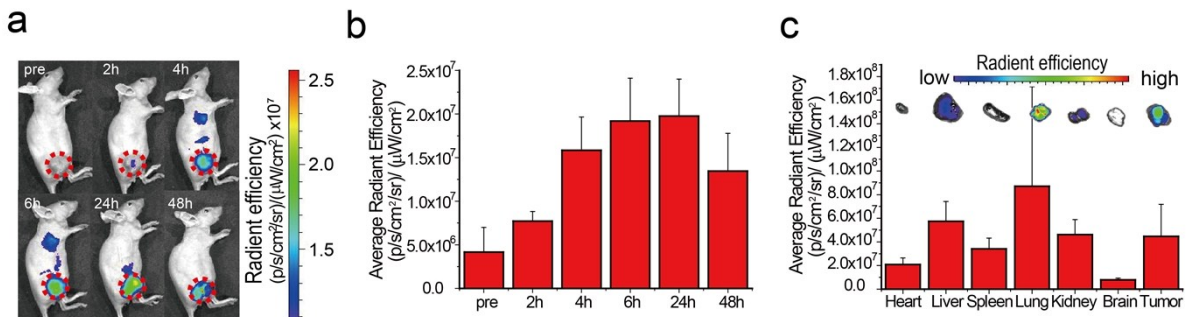


Figure S12. a) *In vivo* fluorescence images and b) corresponding fluorescence intensity of nude mice after tail vein injected of free IR780 over time. The tumors were indicated with red circles. c) *Ex vivo* biodistribution and relative quantitative analysis of free IR780 in major organs after 48 h. Values are the means \pm SD (n = 3).

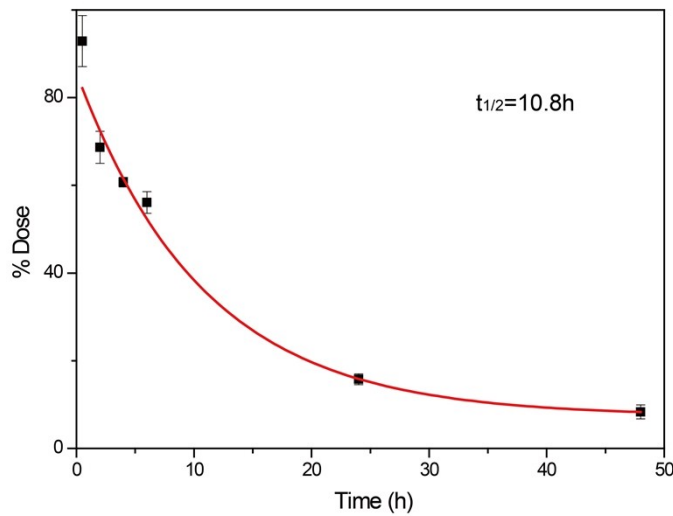


Figure S13. Blood clearance of LIP-IR-CAT measured by a fluorescent spectrophotometer up to 48 h post intravenous injection. Values are the means \pm SD (n = 5).

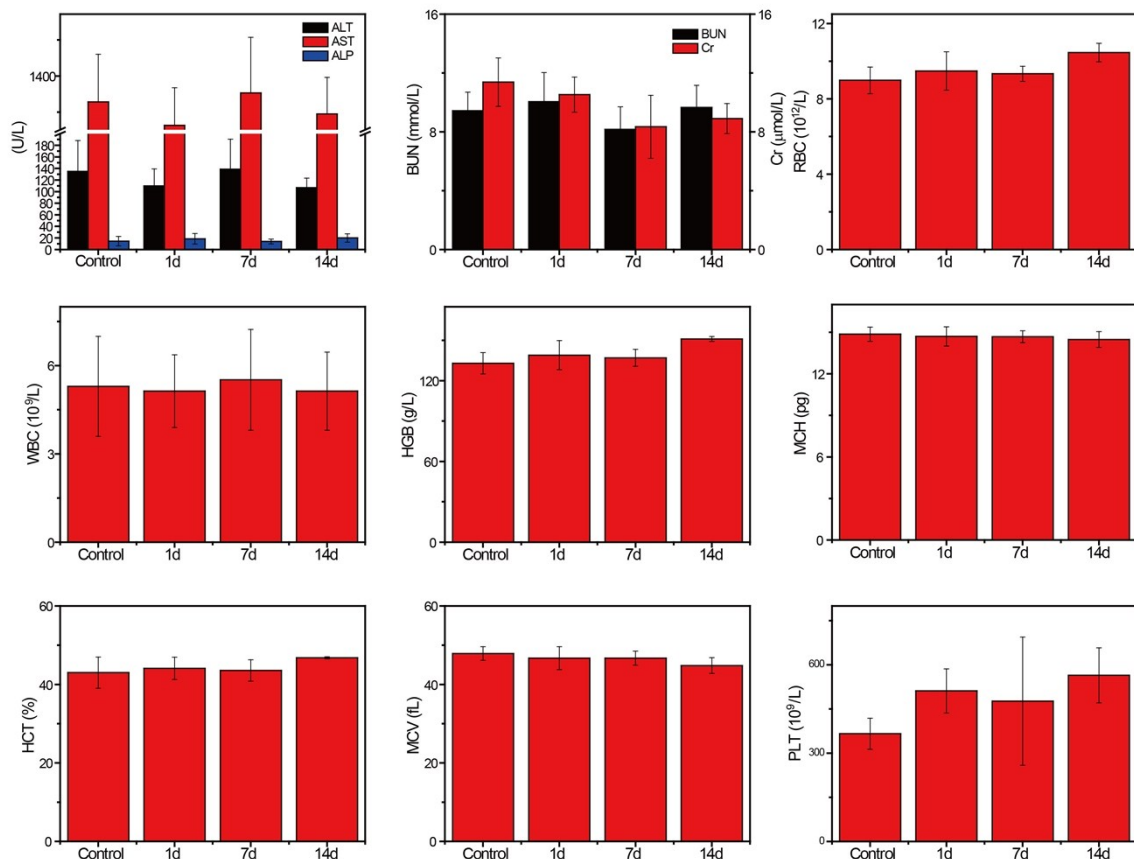


Figure S14. Blood biochemistry and complete blood analysis of Kunming mice after intravenous injection of LIP-IR-CAT (2 mg/mL, PBS as control) at the various time points (1st, 7th, and 14th day). The examined parameters included alanine aminotransferase (ALT), aspartate aminotransferase (AST), alkaline phosphatase (ALP); blood urea nitrogen (BUN); creatinine (Cr); red blood cell (RBC) counts; white blood cell (WBC) counts; hemoglobin (HGB); mean corpuscular hemoglobin (MCH); hematocrit (HCT); mean corpuscular volume (MCV) and platelets (PLT). Values are the means \pm SD (n = 5).

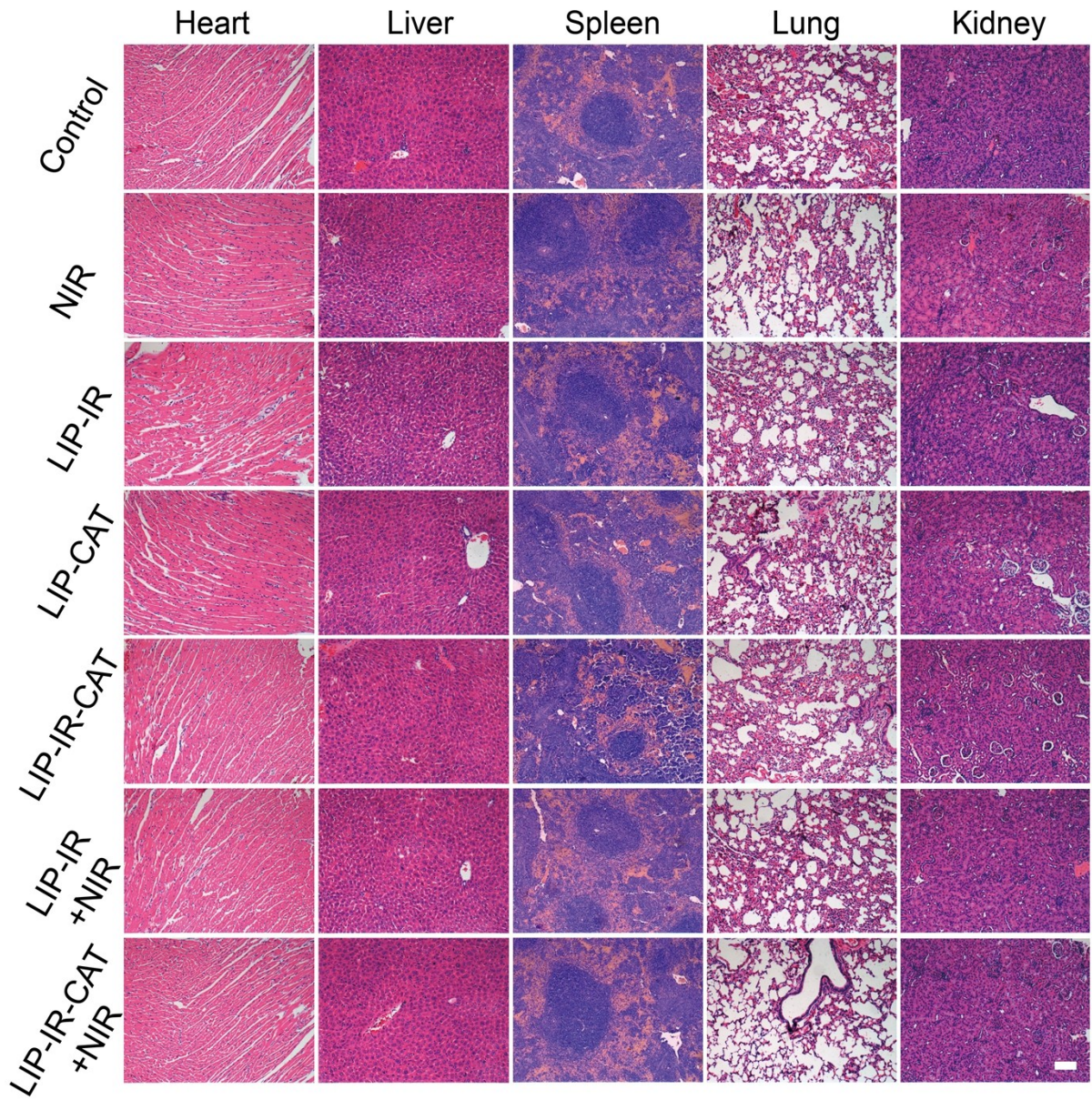


Figure S15. HE-stained tissue sections of major mice organs (heart, liver, spleen, lung, and kidney) on the 14th day after different treatments. Saline-treated mice were used as the control. Scale bar: 200 μ m.

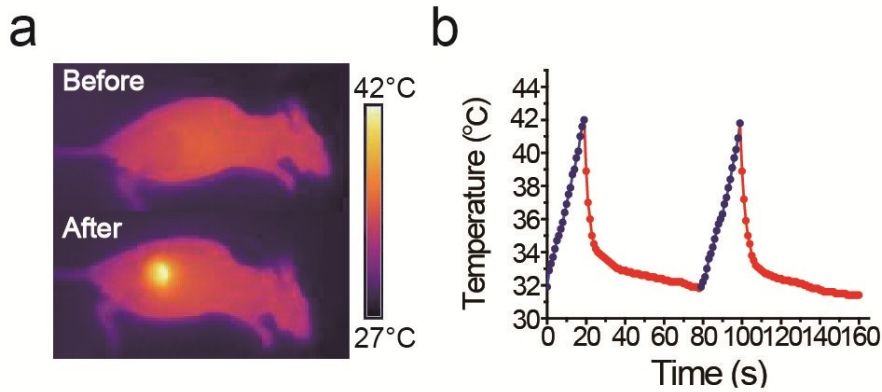


Figure S16. a) Infrared thermal images and b) the relative temperature variation of mice intravenous injected with LIP-IR-CAT before and after an 808 nm laser irradiation (1.5 W/cm², 20 s twice with 1 min interval).

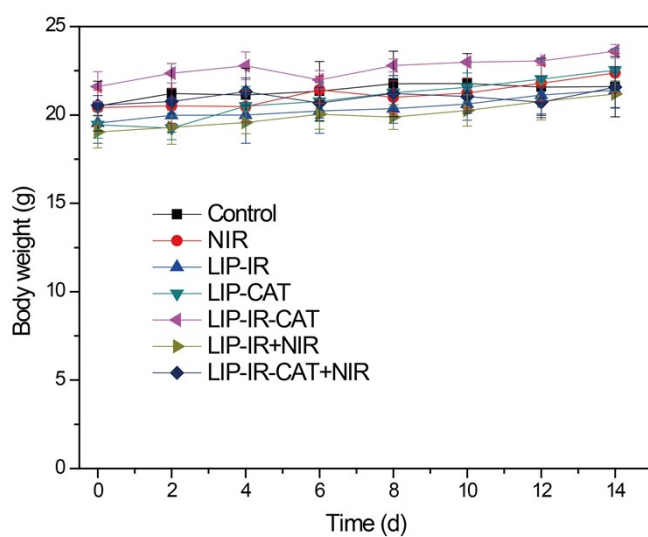


Figure S17. Body weights of MDA-MB-231 tumor-bearing nude mice in different groups over the 14 days. (mean ± SD, n = 5).

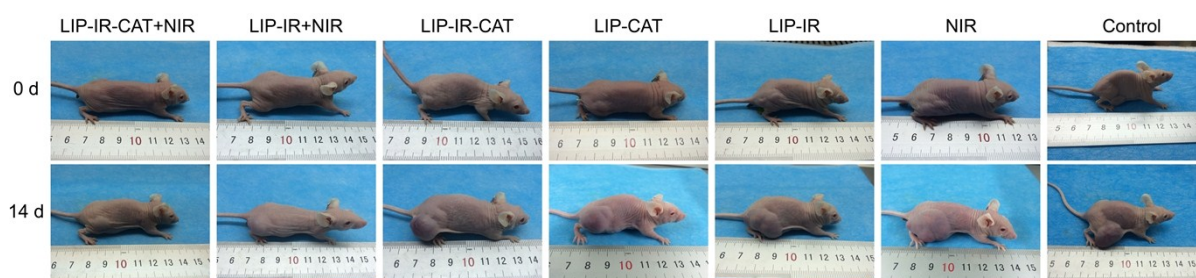


Figure S18. The photos of mice bearing MDA-MB-231 tumor under different treatments.